IEEE Access
Multidisciplinary ⋮ Rapid Review ⋮ Open Access Journal

Received 30 April 2025, accepted 3 June 2025, date of publication 9 June 2025, date of current version 3 July 2025.

Digital Object Identifier 10.1109/ACCESS.2025.3577747

RESEARCH ARTICLE

Modeling and Simulation of Backlash Dynamics of Worm-Wheel System and Its Gap Size Estimation Using Kalman Filters

ABERA TULLU[1], (Member, IEEE), JIHYOUNG CHA[2], (Member, IEEE), AND SANGHO KO[1], (Member, IEEE)

[1]Department of Smart Air Mobility, Korea Aerospace University, Goyang 10540, Republic of Korea
[2]Centre for Aeronautics, Cranfield University, MK43 0AL Cranfield, U.K.

Corresponding author: Sangho Ko (sanghoko@kau.ac.kr)

This work was supported in part by the Ministry of Trade, Industry and Energy (MOTIE), South Korea; and in part by Korea Evaluation Institute of Industrial Technology (KEIT) through the Technology Development Program under Grant 20015920.

ABSTRACT Reduced weight, size, and maintenance cost, as well as quieter and eco-friendly operation of electro-mechanical actuators (EMA), gained profound attention in various sectors, particularly aerospace. As a result, hydraulic actuators are being replaced by EMA counterparts. However, EMA comprises mating gear systems used for power transmission, and these gears experience wear through time. Among widely known EMAs variants, worm-wheel gear system is quietest, smoothest, and compact with high gear ratio. Due to these advantages, worm-wheel is utilized in various devices that require high precision such as surgical robotic arms and 3D printers. Nevertheless, worm-wheel systems, alike other variants of mating gear systems in EMA, suffer friction wear that leads to a backlash in the system. Backlash induces non-linearity in the dynamics of the worm-wheel system, resulting in reduced EMA performance and complex control system design. Therefore, as a part of EMA prognostic and health management (PHM) approaches, we develop a mathematical model of the non-linear dynamic behavior of backlash in the worm-wheel system and derived equations from the model for backlash gap size estimation. This backlash gap size estimation can be employed not only for monitoring of worm-wheel system performance and reliability as a proactive measure but also for its compensation control system design. Simulations of backlash dynamic behavior and gap size estimation were conducted using the Matlab/simscape tool. Extended and unscented Kalman filters were implemented to estimate backlash gap size, and their performance was compared using root-mean-square error technique. Results show that both Kalman filters estimate a simulated gap size very well. However, the unscented Kalman filter performs relatively higher than that of the extended Kalman filter around sharp edges during the switching behavior.

INDEX TERMS Electro-mechanical actuator (EMA), worm-wheel system, backlash dynamics, Kalman filters, prognostic and health management (PHM).

I. INTRODUCTION

With the advent of electro-mechanical actuators and emergence of their remarkable advantages [1], [2], [3] over hydraulic actuators, widely used in aircraft control systems, there has been a significant shift in the aerospace sector towards fully implementing electric-based actuation systems to acquire those advantages. However, EMA comes with challenges, such as the incursion of backlash, which induces non-linearity in the control system and reduces performance. The existence of backlash in the mating gear system is due to multiple factors such as manufacturing or assembly error [4], [5], friction-induced teeth wear-out [6], compensation for expansion of mating gears at high temperatures, or intentionally introduced for ease of mating gear play [7]. Regardless, backlash degrades power

The associate editor coordinating the review of this manuscript and approving it for publication was Jesus Felez.

2025 The Authors. This work is licensed under a Creative Commons Attribution 4.0 License.
For more information, see https://creativecommons.org/licenses/by/4.0/

transmission system and incurs challenges to control systems designs which precisely position aircraft control surfaces, retraction/extension of landing gears or other steerable components.

Over the years, various approaches have been deviced to monitor wear in mating gear systems that leads to backlash. A compressive review on mating gear systems health monitoring approaches was given by Anusha et al. [9]. Among the state-of-the-art methodologies for mating gear system health monitoring, vibration analysis approach is widely reported [10], [11], [12], [13]. Digital twin and data driven techniques are also becoming key methodologies for the health monitoring [14], [15], [16].

To address the challenges induced by backlash, multiple research works have been reported, which, in general, can be categorized into backlash gap size and control system design for backlash compensation. Badr et al. [18] considered gear backlash as integral of random white noise and employed Kalman filter to estimate its gap size. Bahdir et al. [19] developed and experimentally validated a software tool that estimated the minimum and maximum gap sizes in mating gear system. A time domain approach that automatically estimates backlash gap size based on sensor information was proposed by Christian et al. [20]. Shiva et al. [21] deviced a generic method named ''backlash energy'' that estimates backlash size based on motion data such as position and velocity of the rotating gears. According to the authors report, the presence of backlash induces gear misalignment in the mating gear system and that misalignment causes localized energy. Based on this energy, the authors estimated backlash gap size. Mattias et al. [22] proposed a simple model for backlash size estimation base on phase plane analysis.

Progresses have been made in the control system design for mating gear systems with backlash. Mattias and Per-Olof [23] conducted a survey on some of the linear and nonlinear control systems designed to compensate the effect of backlash in the dynamics of mechanical systems. Jaisheela and Kumar [24] proposed two approaches for the compensation of backlash in EMA. One of the approach is simulation based while the other is design based. In the simulation based approach, a simple partial derivative (PD) controller was designed and simulink optimization toolbox was employed to tune the parameters of the controller. In the design approach, the authors proposed increasing friction between the mating gears' surfaces to compensate for the backlash. Prasanga et al. [25] also proposed a method that compensates backlash in actuator system of a robot. The method utilizes identical counter-operating drives at each joint of the robot. Kalantari and Foomani designed adaptive algorithm that eliminates backlash in mating gear system based on the system's angular position error.

Mating gears in EMA have different forms, and the estimation and compensation approaches to their backlashes differ. Though there are many gear sets, the commonly known and widely used gear set types are spur, bevel, and worm-wheel. The choice of a particular mating gear set type depends on the desired application. Worm-wheel gear set is often preferred over other gear set variants due to its smooth power transmission, high gear reduction ratio in a single step hence compact, and self-locking capability to avoid unintended reverse motion due to the reaction of a driven component. This gear set is used in many areas, such as robotics [27], [28], [29], [30], the aerospace sector for precise deflection of aircraft control surfaces and landing gear steering [31], smooth and accurate control of solar panels [32] and so on.

In worm-wheel systems, power transmission from worm to wheel is possible only through the sliding motion of wheel teeth over worm thread or vice-versa. Lubricant is injected into the contacting surfaces to reduce friction between the thread and teeth. Thicker lubricants avoid surface contact between the worm and the wheel. However, a study by Hardik et at. [33] shows that the worm-wheel system suffers significant churning power loss due to lubricant-induced drag. Thin lubricants are easily rubbed off the mating thread and teeth, resulting in sliding friction between the two surfaces. Regardless of lubricants, teeth wear due to friction exists, and the incursion of backlash in the worm-wheel gear set is imminent.

Eliminating backlash in the worm-wheel systems is difficult. However, numerous research works have been done on reducing the backlash gap size or compensating for its presence through control system designs to improve power transmission efficiency. Adjusting the center distance between mating gears and utilizing gear teeth with less thinning are simple techniques for reducing backlash gap size. Wojciech et al. [34] proposed a method of reducing backlash size between worm thread and wheel teeth utilizing an adaptive worm in its axial direction and deformable wheel rim. In their other work, Wojciech et al. [35] proposed adjustable backlash through a special worm and wheel teeth design.

The worm-wheel system operates with high sliding friction between the worm thread and wheel teeth, so it suffers from wear that leads to increased backlash. Estimating the backlash size is therefore essential to further device methodologies that take this size into consideration for efficient power transmission performance. The plausible methodologies include monitoring performance as gap size increases over time. This approach enables system prognosis and in-operation health monitoring, reducing system repair and maintenance downtime [36], [37], [38].

With the core importance of backlash estimation, this work focused on developing a mathematical model that depicts the non-linear dynamic behavior of backlash in the worm-wheel system from which backlash gap size can be estimated. This estimation enables control system design for the compensation of the backlash resulting in higher precision and repeatability in positioning which are essential in industrial and surgical robotic arms manipulation, 3D printers, CNC machines, satellite antenna positioning, missile guidance systems, and other industrial machineries such as elevators and heavy-duty gearboxes.

To the author's knowledge, there is no prior research work reported on a derivation of mathematical model that predicts the dynamics and estimates backlash gap size in a worm-wheel gear set. There are research works on mathematical modeling of backlash in spur gear sets [20], [39], [40], but the dynamics of such gear sets are quite different from that of worm-wheel gear sets. Yeh et al. [41] developed a mathematical model to analyze the modeling and control issues related to worm-wheel but with the assumption that there is no backlash in the worm-wheel system.

Details of the work presented in this paper are sectioned as follows. In Section II, challenges in worm-wheel systems are stated, and a proposed approach to resolve these challenges is described. Worm gear dynamics and backlash estimation formulations are presented in Section III. Estimation techniques such as extended and unscented Kalman filters are utilized in Section IV for backlash size estimation, followed by Matlab simscape modeling and simulations presented in Section V. Results and discussions are given in Section VI, and the conclusion is given in Section VII.

II. PROBLEM STATEMENT AND METHODOLOGY

Despite its exceptional advantages, the worm-wheel system is prone to power loss due to various factors [8]. Friction-induced wear, overheating, and lubricant oil leaking. Sliding friction between worm thread and wheel teeth surfaces accounts for a significant amount of power loss. This friction causes wheel teeth to wear as the wheel is often made from materials susceptible to wear compared to worms. Since backlash due to wear of teeth is imminent, online monitoring of the power transmission performance of the system is a conceivable approach to taking proactive measures [14].

Therefore, we propose a mathematical-model based estimation of backlash gap size in a worm-wheel system that can be used to monitor the system's performance, hence reliability, and to design a control system that compensates the estimated gap. A mathematical model that describes the dynamics of backlash is required to estimate gap size. The dynamic model is then modified to a state-space model so that the backlash gap size, as one of the state variables, can be estimated through well-known techniques such as Extended and Unscented Kalman filters. The accuracy of these filters in estimating the gap size is compared and the best method is recommended.

The backlash gap size is the maximum relative displacement that the worm thread makes before it makes contact with subsequent teeth of the wheel and vice-versa. In the state-space model, the backlash gap size varies between consecutive contacts of worm thread and wheel teeth. The relative position of this varying size at any time is taken as one of the state variables of the state-space model. The relative velocity and coefficient of friction between worm thread and wheel teeth are considered as the other state variables of the state-space model.

The coefficient of friction is an unobservable state variable. Therefore, an equation is formulated to predict its evolution, and the unscented Kalman filter is utilized to estimate its value. The estimated value is then augmented with the other state variables: relative position and velocity. The augmented state variables are then fed to unscented and extended Kalman filters through which backlash gap size is estimated. This estimation process is summarized in Fig. 1.

III. DYNAMICS OF WORM-WHEEL SET

The development of a mathematical model for backlash estimation refers to a worm-wheel system of EMA shown in Fig. 2. To illustrate the worm-wheel system setup, a schematic diagram is given in Fig. 3a. Referring to this figure, a normal force F_n acts on the worm thread by wheel tooth. This force induces a frictional force f tangent to the worm thread surface.

Referring to the Cartesian coordinate system shown in Fig. 3a, where y points out of the page, the components of the normal force F_n acting on the worm are

$$\begin{aligned} F_x &= \pm F_n \cos\phi \cos\lambda - f \sin\lambda, \\ F_y &= \mp F_n \cos\phi \sin\lambda - f \cos\lambda, \\ F_z &= -F_n \sin\phi, \end{aligned} \tag{1}$$

where the upper and lower operators ($\pm$ and $\mp$) in front of F_n represent left and right contact, respectively, between the worm thread and wheel teeth, as shown in Fig. 3b. The variables λ and ϕ are the worm's lead angle and the wheel's pressure angle, respectively. The lead angle is the angle that a line tangent to the thread surface makes with the plane perpendicular to the axial direction of the worm, and the pressure angle is the angle between the normal force F_n and the line tangent to the pitch circle at the point of contact.

During surface-to-surface contact between the worm and the wheel, the friction force f is related to normal force F_n as $f = \mu F_n$, where μ is the coefficient of sliding friction. Due to sliding friction, the wheel teeth wear-out (reduce in width) and hence induce backlash, which leads to a delay in consecutive contacts between the worm thread and the wheel teeth. As shown in Fig.3b, the delay is represented by extra displacement (x) that the worm thread has to make to contact the next wheel tooth. A mathematical derivation that relates this delay with the backlash gap in the worm-wheel system is given in section III-A, and our purpose is to estimate the backlash due to teeth wear-out.

Let a motor torque (τ_1) be applied on the worm, and an external torque (τ_2) be imposed on the wheel, as shown in Fig.3a. The dynamic equations of the worm and wheel, respectively, are

$$\begin{aligned} J_1\ddot{\theta}_1 &= \tau_1 + (\pm F_n \cos\phi \sin\lambda - f\cos\lambda)\, r_1, \\ J_2\ddot{\theta}_2 &= \tau_2 - (\pm F_n \cos\phi \cos\lambda + f\sin\lambda)\, r_2, \end{aligned} \tag{2}$$

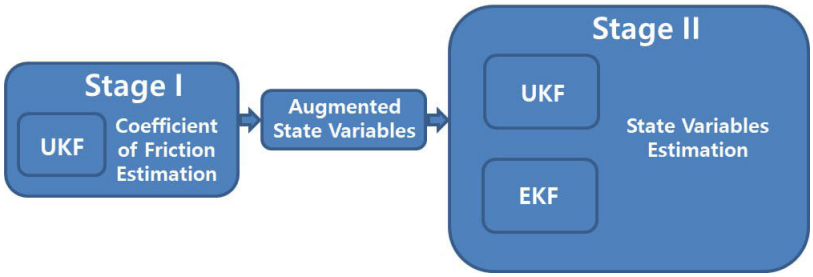

FIGURE 1. State estimation stages.

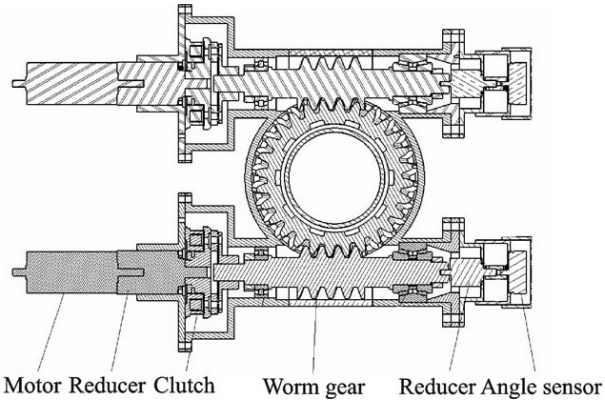

FIGURE 2. EMA with a worm-wheel gear set [31].

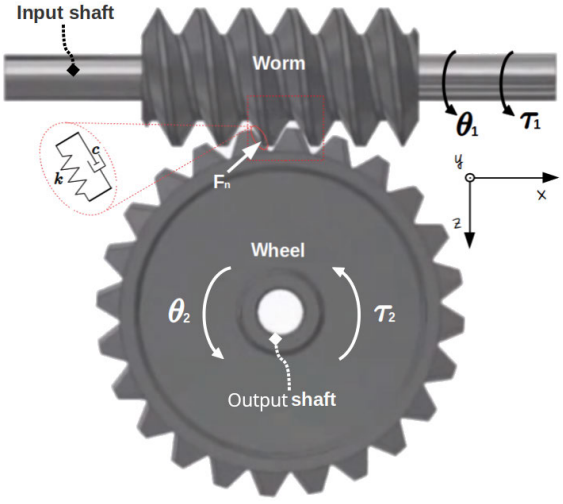

(a) Worm-wheel set

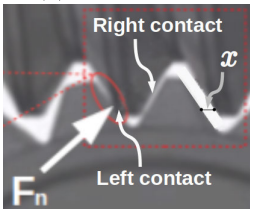

(b) Tooth worn-out and contact delay

FIGURE 3. Schematics of worm-wheel set.

where J_i, θ_i, and r_i, for $i = 1, 2$, are the mass moment of inertia, angular displacements, and pitch radii of the worm and the wheel, respectively.

A. BACKLASH MODEL

In the absence of backlash, theoretically, the dynamics of the worm-wheel system maintains the transmission ratio expressed as $\theta_1 = \Gamma_{12}\theta_2$, where Γ_{12} is the transmission ratio. However, the thinning of wheel teeth delays consecutive teeth-thread contacts, and the transmission ratio can not be maintained. This delay (x) is quantified as a fraction of worm lead that the worm has to be displaced by before the next thread-tooth contact is commenced. The lead (l_1) of a worm is the axial distance a point on the thread transverses for one complete revolution of the worm. The length of the delay (x) is quantified as a fraction of l_1. The derivation for this delay is given as follows.

$$\begin{aligned} l_1 &= 2\pi r_1 \tan\lambda, \\ x_1 &= \theta_1 r_1 \tan\lambda, \end{aligned} \tag{3}$$

which gives

$$x_1 = \frac{l_1}{2\pi}\theta_1, \tag{4}$$

where θ_1 is a fraction of 2π. A linear displacement x_2 of the wheel is related to angular displacement(θ_2) and pitch radius r_2 of the wheel as

$$x_2 = r_2\theta_2, \tag{5}$$

Let a relative displacement of the wheel with respect to the worm is defined as

$$x = x_2 - x_1 + b. \tag{6}$$

where x is the relative displacement, and b is a variable to be determined using a constraint that calibrates x. For this relative displacement x to represent backlash, it has to be calibrated as follows. Using Eq.4 and Eq.5, Eq.6 can be re-written as

$$x = r_2\theta_2 - \frac{l_1}{2\pi}\theta_1 + b. \tag{7}$$

In the absence of backlash ($x = 0$), the transmission ratio of the two worms has to be maintained ($\theta_1 = \Gamma_{12}\theta_2$). Substituting these premises into Eq.7, the variable b is expressed as

$$b = (\frac{l_1\Gamma_{12}}{2\pi} - r_2)\theta_1. \tag{8}$$

Combining Eq.7 and Eq.8, the backlash is expressed as

$$x = \frac{l_1}{2\pi}(\Gamma_{12}\theta_2 - \theta_1). \tag{9}$$

The above equation describes the magnitude of circumferential shake that the wheel can make while the worm is kept constant or an axial shake that the worm makes along x-axis if the wheel is fixed. In the case when $\theta_1 = \Gamma_{12}\theta_2$, the shakes are zero, and hence there is no backlash. Henceforth, relative displacement and backlash are used interchangeably.

The second-order derivative of relative displacement x with respect to time has the form

$$\ddot{x} = \frac{l_1}{2\pi}(\Gamma_{12}\ddot{\theta}_2 - \ddot{\theta}_1). \tag{10}$$

where $\ddot{\theta}_2$ and $\ddot{\theta}_1$ are angular accelerations of the wheel and the worm, respectively and $\ddot{x}$ is a linear relative acceleration between the wheel and the worm. The dynamics equations of the worm and the wheel, given in Eq.2 can be re-written as

$$\begin{aligned} \ddot{\theta}_1 &= \frac{1}{J_1}\left[\tau_1 + (\pm F_n \cos\phi \sin\lambda - f\cos\lambda)\, r_1\right], \\ \Gamma_{12}\ddot{\theta}_2 &= \frac{\Gamma_{12}}{J_2}\left[\tau_2 - (\pm F_n \cos\phi \cos\lambda + f\sin\lambda) r_2\right]. \end{aligned} \tag{11}$$

Referring to Eq.10 and Eq.11, the dynamics of worm-wheel system is generalized to

$$\ddot{x} = \begin{cases} \alpha\left[u + F_n\gamma_1\cos\phi + f\gamma_2\right], & \text{left contact}, \\ \alpha\left[u - F_n\gamma_1\cos\phi + f\gamma_2\right], & \text{right contact}, \end{cases} \tag{12}$$

where the following definitions were made

$$\begin{aligned} \alpha &:= \frac{l_1}{2\pi J_1 J_2}, \\ u &:= \Gamma_{12}J_1\tau_2 - J_2\tau_1, \\ \gamma_1 &:= r_2\Gamma_{12}J_1\cos\lambda + r_1 J_2\sin\lambda, \\ \gamma_2 &:= r_1 J_2\cos\lambda - r_2 J_1\Gamma_{12}\sin\lambda. \end{aligned} \tag{13}$$

The normal force F_n causes torsional and compressive stress on a lubrication film infused between worm thread and wheel teeth. Reacting to the stress, the film imposes stiffness and viscous damping on the system's dynamics. As shown in Fig. 3a, these effects are modeled by the spring and damper system at the point of contact. The mathematical equation that represents this phenomenon is given as

$$F_n = kx + c\dot{x}, \tag{14}$$

where k and c are coefficients of elastic stiffness and damping of lubrication film, respectively. During the relative sliding of worm thread with respect to wheel teeth, the friction force f in Eq. 12 has two forms: friction due to viscous damping and friction due to Coulomb damping. The torsional stress imposes shear deformation on the film before the onset of sliding friction, after which the surfaces of the worm thread and wheel teeth are in contact. It is at this point where viscous damping is replaced by Coulomb damping. When the contacted surfaces are separated, the lubricant is injected into them, and hence, the process of damping is re-cycled between viscous and Coulomb. In both damping cases, the friction force f is proportional to the normal force F_n: the higher the normal force is, the stronger the torsional stress and sliding friction are. Therefore, the friction force is equated as

$$f = \mu_d F_n, \tag{15}$$

where μ_d represents the coefficient of both viscous and Coulomb dampings. It is a parameter whose value varies from zero, when there is no contact between worm thread and wheel teeth, to non-zero, when the two bodies are in contact. A coefficient of friction between two bodies in contact depends on the relative speed of one body with respect to the other [42]. The dependency of the coefficient of friction on the relative velocity is formulated as follows:

$$\mu_d = \epsilon\left(\mu_k + (\mu_s - \mu_k)e^{-\dot{x}}\right), \tag{16}$$

where μ_s and μ_k are coefficients of static and kinetic frictions, respectively. The value of this damping coefficient is estimated using an unscented Kalman filter, as described later in the simulation section. The parameter ϵ takes either 0 or 1. When there is no contact between the worm thread and the wheel tooth, $\epsilon = 0$; when there is contact, $\epsilon = 1$.

Substituting Eq.14 into Eq.12 and re-arranging terms, the general dynamic equation is expressed as

$$\ddot{x} = \begin{cases} \alpha\left[u + (kx + c\dot{x})(\mu_d\gamma_2 + \gamma_1\cos\phi)\right], & \text{left contact} \\ \alpha\left[u - (kx + c\dot{x})(\mu_d\gamma_2 + \gamma_1\cos\phi)\right], & \text{right contact} \end{cases} \tag{17}$$

The dynamic equation in Eq.17 is satisfied when the worm and wheel are in either right or left contact. If the worm and wheel are not in contact, the normal force F_n and hence the friction force f are zero. The dynamic equation is then modified as

$$\ddot{x} = \alpha u. \tag{18}$$

The three conditions of worm-wheel dynamics, given in Eq. 17 and Eq. 18 can be re-written as

$$\ddot{x} = \begin{cases} \alpha\left[u + (kx + c\dot{x})(\mu_d\gamma_2 + \gamma_1\cos\phi)\right], & \text{left contact} \\ \alpha u, & \text{no contact} \\ \alpha\left[u - (kx + c\dot{x})(\mu_d\gamma_2 + \gamma_1\cos\phi)\right], & \text{right contact.} \end{cases} \tag{19}$$

The compact form of these equations is given as

$$\ddot{x} = \alpha\left[u + \epsilon\,(kx + c\dot{x})(\mu_d\gamma_2 + \gamma_1\cos\phi))\right], \text{ where}$$
$$\epsilon = \begin{cases} 1, & \text{for} \quad |\,x\,| \geq x_b, \\ 0, & \text{for} \quad |\,x\,| < x_b. \end{cases} \tag{20}$$

Here, x_b is half of the backlash gap size.

B. STATE-SPACE MODEL

The selected state variables of the dynamic model are the relative displacement x, the relative velocity $\dot{x}$, and the coefficient of damping friction μ_d from which state vector ($\mathcal{X}$) is defined as $\mathcal{X} := [x \quad \dot{x} \quad \mu_d]^T$. The observable (measurable) state

variables are x and $\dot{x}$. The state variable μ_d is predicted from the relative velocity.

For the state-space model, the dynamic equation of motion of the worm-wheel system given in Eq.20 is reduced to first-order differential equations. By defining:

$$x_1 := x, \qquad x_2 := \dot{x}, \qquad \text{and} \qquad x_3 := \mu_d,$$

we have

$$\begin{aligned} \dot{x}_1 &= x_2, \\ \dot{x}_2 &= \alpha \left[u + \epsilon(kx + c\dot{x})(\mu_d \gamma_2 + \gamma_1 \cos\phi)\right], \\ \dot{x}_3 &= 0. \end{aligned} \tag{21}$$

Eq.21, along with the measurement output $\mathcal{Y} = [x_1 \quad x_2]$, can be expressed in a compact form as

$$\begin{aligned} \dot{\mathcal{X}} &= \mathfrak{F}(x, \dot{x}, \mu_d, u) + w, \\ \mathcal{Y} &= \mathfrak{h}(x, \dot{x}) + v, \end{aligned} \tag{22}$$

where $\dot{\mathcal{X}} = [\dot{x}_1 \quad \dot{x}_2 \quad \dot{x}_3]^T$, and $\mathfrak{F}$ is a vector valued function of the form

$$\mathfrak{F} = \begin{bmatrix} \mathfrak{F}_1 \\ \mathfrak{F}_2 \\ \mathfrak{F}_3 \end{bmatrix} = \begin{bmatrix} \dot{x} \\ \alpha \left[u + \epsilon(kx + c\dot{x})(\mu_d \gamma_2 + \gamma_1 \cos\phi)\right] \\ 0 \end{bmatrix}, \tag{23}$$

and w and v are process and measurement noises, respectively.

IV. BACKLASH ESTIMATION

In general, the evolution of the dynamic system and its measurement using sensors suffer process and measurement uncertainties (noises) that need to be filtered out for precise estimation of the evolving variables. In this work, the extended and unscented Kalman filters [43] are used to filter out noises from the evolving variables known as state variables and estimate their values.

The angular positions and velocities of the worm and wheel are observable state variables from which the relative linear displacement (x) and velocity ($\dot{x}$) are obtained. The coefficient of friction μ_d is augmented with x and $\dot{x}$ as an additional state variable. The augmented state vector is then estimated using the filters mentioned above. The non-zero coefficient of friction can have a static or kinetic phase. In the simulation, we considered the extreme values of this parameter to be between zero and a value of static coefficient of friction, which is set to be 0.1. However, the coefficient of friction does not simply switch between 0 and 0.1. Once the two surfaces are set to relative displacement, the coefficient of friction reduces from its static value to kinetic, which combines viscous friction due to the lubricant and sliding friction during direct contact between thread and teeth surfaces. The lubricant's viscous friction coefficient is assumed to be 0.08. The unscented Kalman filter estimates its value before augmenting μ_d to x and $\dot{x}$. The process of estimating μ_d is presented in subsection IV-B.

The state variable estimation approach takes two steps in extended and unscented Kalman filters: prediction and update. The value of each state variable is represented by Gaussian distribution (GD) parameterized by mean and covariance matrices. A summary of these steps is given in the following subsections.

A. EXTENDED KALMAN FILTER

In this estimation method, the non-linear dynamic model given in Eq.20 is linearized about operating points, and a linear state-space model is implemented.

The linearized state-space model of non-linear dynamics given in Eq.22, along with output measure, can be given as

$$\begin{aligned} \dot{\mathcal{X}} &= F\mathcal{X} + Gu + w, \\ \mathcal{Y} &= H\mathcal{X} + v, \end{aligned} \tag{24}$$

where F, G, and H are Jacobian matrices of state transformation, control, and output measurement. w is a white Gaussian process noise with zero mean and a covariance matrix Q.

The measurement noise v is represented by a white Gaussian process of zero mean and a covariance matrix R. The Jacobian matrices: F, G, and H are derived as

$$\begin{aligned} F &= \begin{bmatrix} \frac{\partial \mathfrak{F}_1}{\partial x_1} & \frac{\partial \mathfrak{F}_1}{\partial x_2} & \frac{\partial \mathfrak{F}_1}{\partial x_3} \\ \frac{\partial \mathfrak{F}_2}{\partial x_1} & \frac{\partial \mathfrak{F}_2}{\partial x_2} & \frac{\partial \mathfrak{F}_2}{\partial x_3} \\ \frac{\partial \mathfrak{F}_3}{\partial x_1} & \frac{\partial \mathfrak{F}_3}{\partial x_2} & \frac{\partial \mathfrak{F}_3}{\partial x_3} \end{bmatrix} \\ &= \epsilon\alpha \begin{bmatrix} 0 & 1 & 0 \\ k(\gamma_2 x_3 + \gamma_1 \cos\phi) & c(\gamma_2 x_3 + \gamma_1 \cos\phi) & \gamma_2(kx_1 + cx_2) \\ 0 & 0 & 0 \end{bmatrix}, \\ G &= \begin{bmatrix} \frac{\partial \mathfrak{F}_1}{\partial \tau} \\ \frac{\partial \mathfrak{F}_2}{\partial \tau} \\ \frac{\partial \mathfrak{F}_3}{\partial \tau} \end{bmatrix} = \begin{bmatrix} 0 \\ \alpha \\ 0 \end{bmatrix}, \quad \text{and} \\ H &= \begin{bmatrix} \frac{\partial \mathfrak{h}_1}{\partial x_1} & \frac{\partial \mathfrak{h}_1}{\partial x_2} & \frac{\partial \mathfrak{h}_1}{\partial x_3} \\ \frac{\partial \mathfrak{h}_2}{\partial x_1} & \frac{\partial \mathfrak{h}_2}{\partial x_2} & \frac{\partial \mathfrak{h}_2}{\partial x_3} \end{bmatrix} = \begin{bmatrix} 1 & 0 & 0 \\ 0 & 1 & 0 \end{bmatrix}. \end{aligned} \tag{25}$$

1) PREDICTION

In the prediction step, the new values of state variables are predicted based on their initial values and the dynamic model. The predicted values are taken as the conditional mean of GD. The variances and covariances of the state variables are also predicted based on initial process noise. The prediction step can be outlined as

$$\begin{aligned} \mathcal{X}^* &= F\mathcal{X} + Gu, \\ P^* &= FPF^T + Q, \end{aligned} \tag{26}$$

where $\mathcal{X}^*$ and P^* are the predicted state vector and the error covariance matrix.

2) UPDATE

In the update step, actual sensor measurements are taken and compared to the predicted values of state variables. The error difference between the measured and predicted values is used with the Kalman gain to update state variables and the error covariance. This update step can be summarized as

$$\begin{aligned} y &= z - \mathfrak{h}(x^*, \dot{x}^*) \qquad \text{where } x^*, \dot{x}^* \in \mathcal{X}^* \\ S &= HP^*H^T + \mathcal{M} \\ K &= P^*H^T S^{-1} \\ &--- \\ \mathcal{X} &= \mathcal{X}^* + Ky \\ P &= (I - KH)P^* \end{aligned} \tag{27}$$

Extended Kalman filter estimates the state of a system by a first-order linearization of nonlinear dynamic equations at consecutive points and hence acheives only a first-order accuracy. This induces error in the posterior values of mean and covariance of state variables. The limitation of this filter lays on the derivation of Jacobean matrices which is often complex to derive, as well. Moreover, to avoid instability in the filter, the time-step interval has to be significantly small hence leads to high computational cost. Despite these drawbacks, extended Kalman filter is widely used in estimating various dynamic systems and parameters.

B. UNSCENTED KALMAN FILTER

The non-linear dynamic model may have sharp changes that the extended Kalman filter may not be able to catch. This may lead to divergence in such estimation methods. As a result, rather than linearizing the non-linear dynamic model, it is better to utilize an unscented Kalman filter to estimate the backlash size. This method represents the value of each state variable of the state model by GD from which sigma points are selected to be predicted and updated. The sigma points are systematically selected, and weights are assigned to them. The number of sigma points and weights depends on the number of state variables. The sigma points ($\mathfrak{d}$) and their corresponding weights ($\mathcal{W}$) are given as

$$\begin{aligned} \mathfrak{d}^0 &= \mathcal{X} \qquad \text{mean of Gaussian,} \\ \mathfrak{d}^i &= \mathcal{X} \pm (\sqrt{(n+\Lambda)P})_i, \\ \mathcal{W}^0 &= \frac{\Lambda}{n+\Lambda}, \\ \mathcal{W}^i &= \frac{\Lambda}{2(n+\Lambda)}, \quad i = 1, 2, 3, \ldots, 2n, \end{aligned} \tag{28}$$

where P and $(\sqrt{(n+\Lambda)P})_i$, respectively, are the process covariance matrix and the i^{th} column of the square-root of the covariance matrix evaluated utilizing the Cholesky decomposition. The sigma points are transformed through the non-linear model of Eq.22 without linearizing it. This makes the unscented Kalman filter popular over the extended Kalman filter. The transformed sigma points do not maintain the GD form, and hence, new ones are generated from the weighted sum of the transformed sigma points as follows.

$$\begin{aligned} \mathcal{X}^* &= \sum_{i=0}^{2n} \mathcal{W}^i \mathfrak{F}(\mathfrak{d}) \\ P^* &= \sum_{i=0}^{2n} \mathcal{W}^i [\mathfrak{F}(\mathfrak{d}) - \mathcal{X}][\mathfrak{F}(\mathfrak{d}) - \mathcal{X}]^T \end{aligned} \tag{29}$$

In the update step, the selected sigma points are transferred through the measurement function $\mathfrak{h}$ as follows

$$\begin{aligned} \mathfrak{z} &= \sum_{i=0}^{2n} \mathcal{W}^i \mathfrak{h}(\mathfrak{d}), \\ S &= \sum_{i=0}^{2n} \mathcal{W}^i [\mathfrak{h}(\mathfrak{d}) - \mathfrak{z}][\mathfrak{h}(\mathfrak{d}) - \mathfrak{z}]^T + Q, \end{aligned} \tag{30}$$

where Q is the measurement noise covariance. The cross-correlation between the state space and measurement space is quantified as

$$T = \sum_{i=0}^{2n} \mathcal{W}^i [\mathfrak{F}(\mathfrak{d}) - \mathcal{X}^*][\mathfrak{h}(\mathfrak{d}) - \mathfrak{z}]^T. \tag{31}$$

The Kalman gain is then determined as

$$K = T \cdot S^{-1}. \tag{32}$$

Using the obtained Kalman gain, the state variables $\mathcal{X}$ and their error covariance P are updated as

$$\begin{aligned} \mathcal{X} &= \mathcal{X}^* + K(z - \mathfrak{z}), \\ P &= (I - KT)P', \end{aligned} \tag{33}$$

where z is the sensor measurement and I is the identity matrix.

Unscented Kalman filter was proposed by Julier and Jeffery [44]. This filter was shown to substantially overcome the limitations of extended Kalman filter. However, the numerical robustness of UKF is influenced by the selection of sigma points and their corresponding weighting parameters [45].

V. SIMULATION

The simulation setup of the worm-wheel system utilizes the Matlab simscape tool. The dynamics of backlash between the worm thread and wheel teeth are introduced to the setup using a rotational hard stop block of simscape with upper and lower bounds. The gap size between these bounds is considered as backlash. In simulation, we assumed this gap size equals a fraction of the worm lead: 10% of l_1 to be specific. This backlash gap is detected during a change in the direction of rotation of a driving body, which in this case is the worm. With the assumed backlash gap and referring to Eq.9, the following relations are obtained:

$$\begin{aligned} 2x_b &= 0.1l_1, \\ \Gamma_{12}\theta_2 - \theta_1 &= 0.2\pi. \end{aligned} \tag{34}$$

Referring to Eq.3 and Table 1, a $0.1l_1$ corresponds to angular rotation $\theta_1 \approx 0.62824$ *rad* of the worm before its thread makes contact with the stationary wheel tooth.

TABLE 1. Mechanical properties of worm and worm wheel [46].

Property	Worm	Worm wheel	Unit
Catalog	SWG2-R1	AG2-20R1	—
Material	S45C	CAC702(AIBC2)	—
Module	2	2	—
Teeth number	single start	20	—
Pitch diameter	31	40	mm
Pressure angle (ϕ)	20	—	degree
Lead angle (λ)	3.69	—	degree
Lead (l_1)	6.28	—	mm
mating distance	—	35.50	mm
weight	0.21	0.26	kg

Rotational motion sensors of the simscape are used to measure angular displacements and velocities of the worm and wheel. The sampling rate of the sensors is set to be 0.002 seconds. The assumed backlash gap size is wide enough for the sensors to acquire samples or measurements of the relative displacements and velocities. The contact at either end of the hard stop is modeled as a surface with stiffness and viscus damper to mimic lubricant film between worm thread and wheel teeth surfaces. The geometric and mechanical properties of the worm and wheel are given in Table 1.

Fig. 4a shows that a pulsed motor torque is applied on the worm while a random external load, shown in Fig. 4b, is applied on the wheel. The net load that drives the worm-wheel system is shown in Fig. 4c. Referring to Eq. 13, the net load is derived from input torque and external load as

$$\tau_{net} = \frac{l_1}{2\pi J_1 J_2}(\Gamma_{12} J_1 \tau_2 - J_2 \tau_1). \tag{35}$$

The overall block structure for state variables estimation is shown in Fig. 5. The worm-wheel system, the EKF, and the UKF for estimating augmented state variables take the net load as a control input. The detailed setup of the worm-wheel system and its sensors is shown in Fig. 6. The system takes in net load as an input and applies it to the worm. The worm-wheel transmission ratio is 20:1, and the backlash gap size between the worm thread and wheel teeth is $0.1l_1$. The rotational sensors 1 and 2 measure the angular displacement and velocity of the worm and wheel, respectively. The corresponding angular displacements and velocities of the two bodies are combined according to the transmission ratio, and then the corresponding relative linear displacement (x_1) and velocity (x_2) are computed.

Before augmenting the coefficient of friction μ_d with the other state variables: x_1 and x_2, its value is predicted using Eq. 16 and estimated using the unscented Kalman filter as shown in Fig. 7. The estimated value of μ_d, represented by x_3, is augmented with the x_1 and x_2 and sent to the extended and unscented Kalman filters for the entire state variables estimation. A detailed explanation of the implementation of an unscented Kalman filter for state and parameter estimation is given by VanDyke et al. [47].

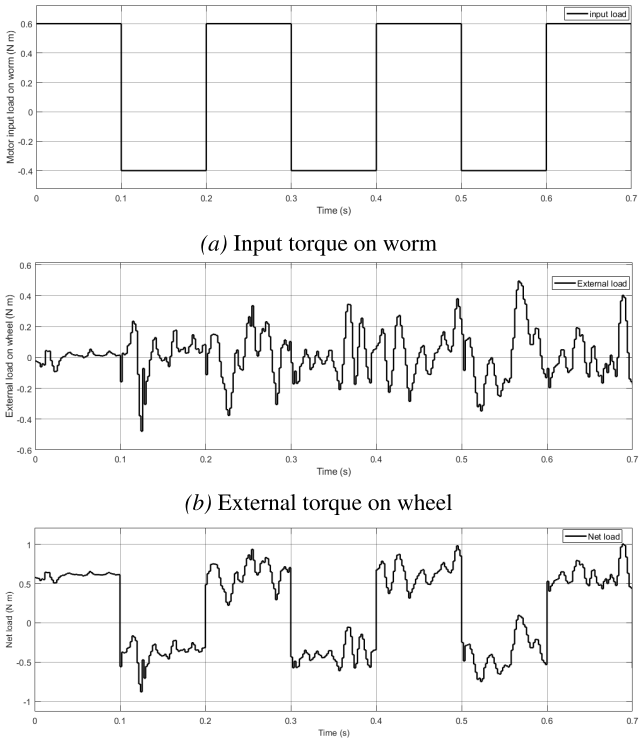

(a) Input torque on worm

(b) External torque on wheel

(c) Net torque on worm-wheel system

FIGURE 4. Applied torque on worm-wheel system.

VI. RESULTS AND DISCUSSIONS

The plots of backlash dynamics and gap estimation are obtained with the simulation setup described in section V. Sensors measurements of angular displacements and velocities of the worm and wheel are shown in Fig. 8. It can be inferred from these plots that the displacement and velocity of the wheel are close to 20 times higher than that of the worm, where 20 is the transmission ratio between the two bodies. In the absence of backlash, the transmission ratio ($\Gamma_{12}\theta_2 = \theta_1$) has to be satisfied. Therefore, the displacement and velocity of the worm should be exactly 20 times that of the wheel.

However, due to the backlash, the dynamics show relative differences in displacements and velocities as shown in Fig.9. The vertical axis of Fig. 9a shows that the relative linear displacement between worm thread and wheel teeth is bounded to a range of -0.315 mm to 0.315 mm. This range represents a backlash gap size ($2x_b$). The worm thread and a wheel tooth are in contact at these extreme ends. While the two bodies stay in contact, the relative displacement remains constant. As a result, the relative velocity becomes zero, as shown in Fig.9b. In response to the net input load, the worm reverses its rotation direction at 0.1 seconds. It switches to a no-contact mode where the relative displacement is no longer constant, and hence, relative velocity increases in proportion to the magnitude of net input torque. The bodies make contact on the other end, where the dynamic behavior repeats.

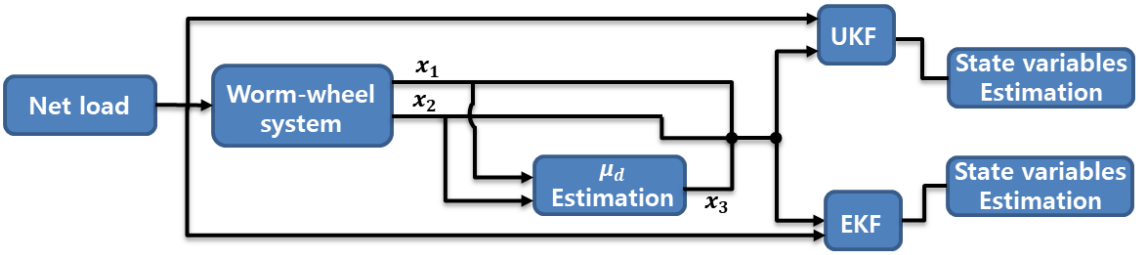

FIGURE 5. Block structure for state variables estimation.

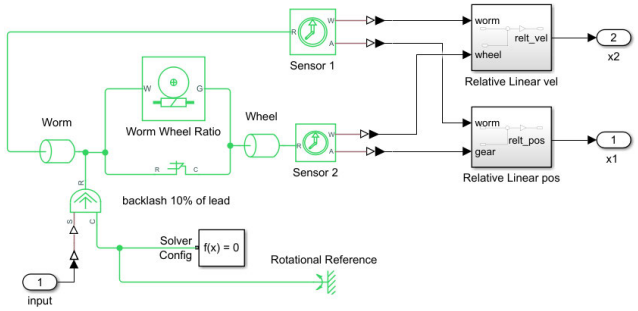

FIGURE 6. Simscape blocks for worm-wheel system.

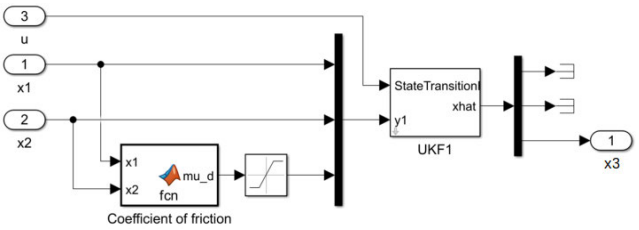

FIGURE 7. Friction coefficient.

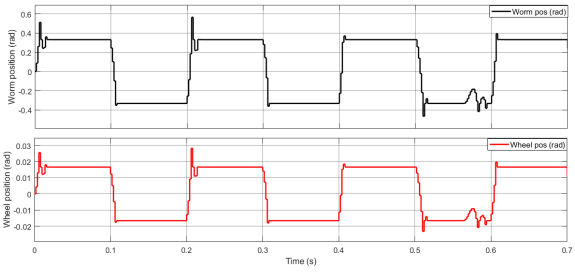

(a) Angular displacements of worm and wheel

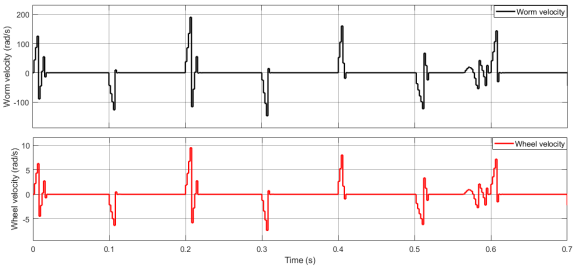

(b) Angular velocities of worm and wheel

FIGURE 8. Displacements and velocities of worm and wheel.

The sharp picks or edges at the instant of contact are due to impact loading delivered by the worm to the wheel.

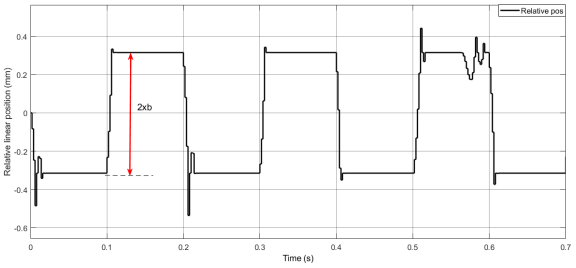

(a) Relative linear position of the wheel

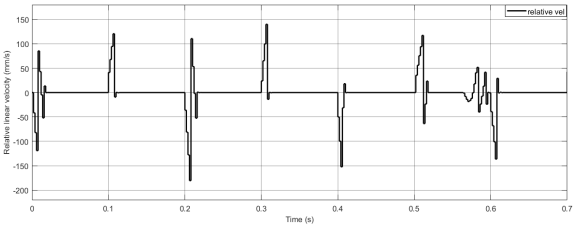

(b) Relative linear velocity of the wheel

FIGURE 9. Relative linear position and velocity of the wheel.

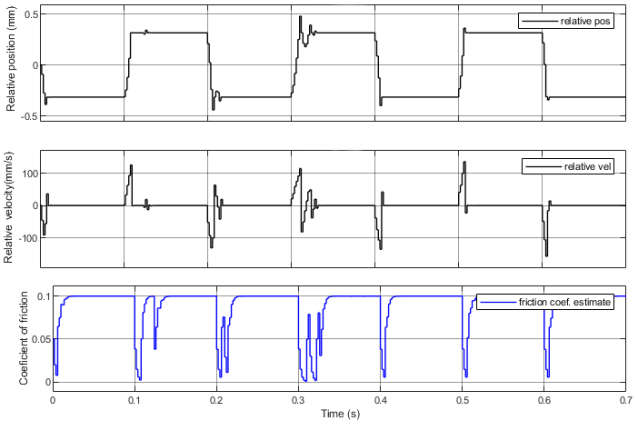

FIGURE 10. Friction coefficient.

The coefficient of friction varies according to relative displacement and velocity, as shown in Fig. 10. When the two bodies are in contact and relative velocity is zero at the extreme ends, the coefficient of friction takes values close to 0.1 (static coefficient of friction). The coefficient of friction drops to zero when there is no contact between the two bodies.

Due to the nonlinearity of the dynamic system, the extended and unscented Kalman filters are utilized to estimate

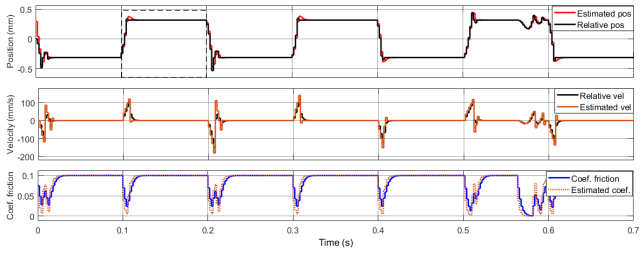

(a) Extended Kalman filter estimation

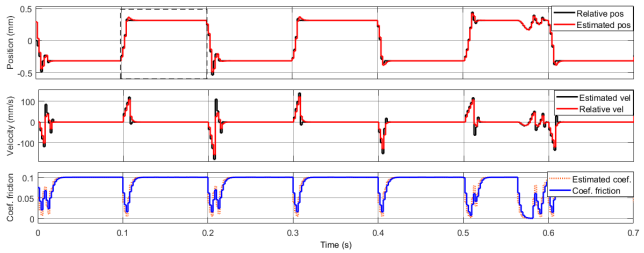

(b) Unscented Kalman filter estimation

FIGURE 11. Extended and unscented Kalman filter estimations.

the state variables. Fig. 11a and Fig. 11b show state estimation by the extended and unscented Kalman filters, respectively. The two filters estimate the state variables very well. However, the unscented Kalman filter outperforms the extended Kalman filter, especially during impacts between the worm thread and wheel teeth.

In the simulations presented in this work, the backlash gap size and the net input torque applied on the worm shaft are assumed. To analyze the sensitivity of the estimators to the changes in these parameters, simulations were conducted for a 10 times increment in the original net input torque and a 50% reduction in the original backlash gap size. These changes were randomly selected to analyze their effects on the gap size estimators. Two simulations were done for the analysis. In the first simulation, the net input torque was increased keeping the original backlash gap size unaltered. For the 10 times increment in net input torque, the original gap size estimation is maintained as shown in Fig.12 showing that the estimtors are not sensitive to a change in net input torque. The relative velocity of the worm gear was increased due to the increase in the net input torque.

In the second simulation, the original net input torque was applied on the worm shaft with worm-wheel backlash gap size reduced. The backlash gap size was reduced by 50% and the original net input torque was applied on the worm shaft to observe an effect on the estimators. As shown in Fig. 13, both the extended and unscented Kalman filters estimated the reduced gap size very well. These analysis show that the employed estimators are not sensitive to changes in the assumed parameters. A more refined sensitivity analysis will be done in the future work.

The accuracy of the extended and unscented Kalman filters in estimating backlash gap size over the time lapse from 0.10 seconds to 0.20 seconds, indicated in Fig.11, is shown in Table 2. Both Kalman filters accurately estimated

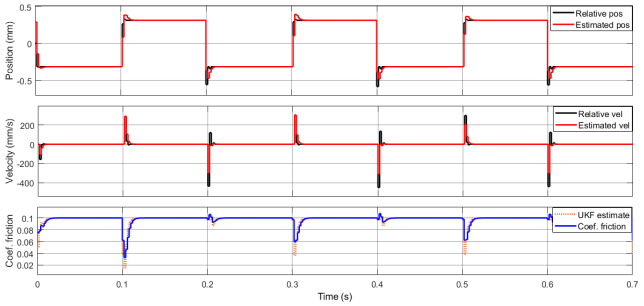

(a) Extended Kalman filter estimation

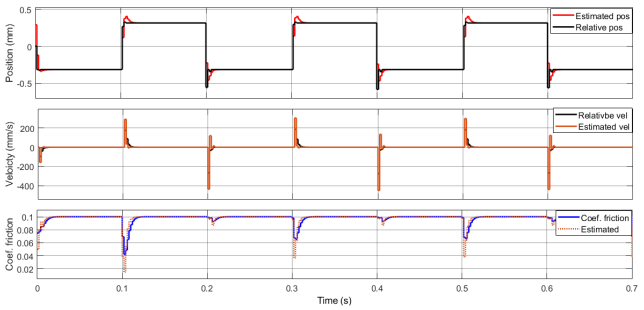

(b) Unscented Kalman filter estimation

FIGURE 12. Estimators sensitivity to a 10 times increment in net input torque.

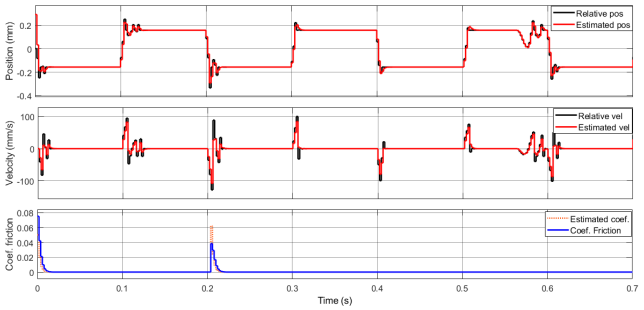

(a) Extended Kalman filter estimation

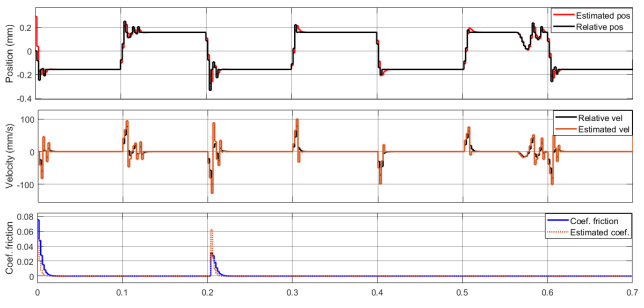

(b) Unscented Kalman filter estimation

FIGURE 13. Estimators sensitivity to 50% reduction in backlash gap size.

the backlash gap size except during impacts between the worm thread and wheel tooth at 0.10 and 0.20 seconds. The unscented Kalman filter performances better than the extended Kalman filter during impacts.

To show the relative difference in the performance of the extended and unscented Kalman filters, their root-mean-square errors are calculated and compared. The plot shown

TABLE 2. Comparison of EKF and UKF performance [46].

Time (s)	True value (mm)	EKF (mm)	UKF (mm)
0.11	0.3150	0.3682	0.3588
0.12	0.315	0.3178	0.3159
0.13	0.3150	0.3177	0.3170
0.14	0.3150	0.3149	0.3150
0.15	0.3150	0.3150	0.3150
0.16	0.3150	0.3150	0.3150
0.17	0.3150	0.3150	0.3150
0.18	0.3150	0.3150	0.3150
0.19	0.3150	0.3150	0.3150

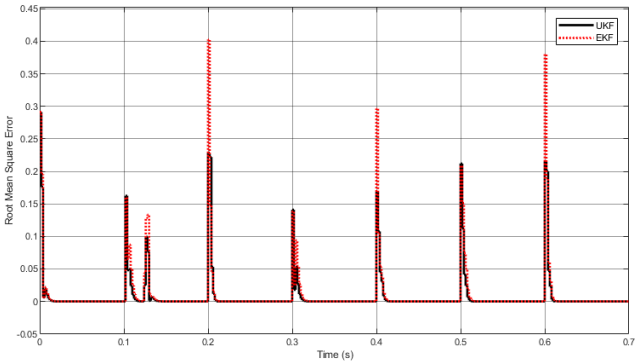

FIGURE 14. Performance of the extended and unscented kalman filters.

in Fig. 14 reflects that the extended Kalman filter has low performance at sharp edges where an abrupt change in system dynamics occurs. The extended Kalman filter estimates the state variables by linearizing the non-linear model and hence can not capture abrupt changes. Unlike the extended Kalman filter, the unscented Kalman filter transforms the nonlinear model as it is and hence captures the system's nonlinearity very well.

VII. CONCLUSION

This study derives a nonlinear dynamics of backlash in a worm-wheel system, from which the backlash gap size is estimated using extended and unscented Kalman filters. The variable coefficient of friction is considered as one of the state variables. The unscented Kalman filter well estimates the variation of this coefficient before its augmentation with the other state variables. The overall state estimation of the utilized Kalman filters is significantly accurate.

In the worm-wheel system, the wheel is made of materials susceptible to friction wear, compared to the worm, and hence requires frequent maintenance or replacement. The developed dynamic model and backlash estimation approach can be considered as an online health monitoring and failure detection means for worm-wheel systems of EMA. Moreover, the derived mathematical model and implemented Kalman filters for estimation of backlash gap size can be used to develop backlash compensation methods in worm-wheel systems to reduce the effect of backlash non-linearity in the control system.

Though the relevance of this work is indispensable in its potential applications, its scope is limited to backlash gap size estimation based on extended and unscented Kalman filters under the assumption of Gaussian noise in both process and measurement. This is done to take advantages of the mathematical tractability and optimality of the Kalman filters. In practical scenario, process and measurement noises are non-Gaussian. Also, in the current work, empirical equation is formulated and unscented Kalman filter is used to estimate coefficient of friction between contacting surfaces of worm and wheel gears. Practically, lubricants are added between mating gears hence the visco-dynamic effect of the lubricant also exists.

In our future work, non-Gaussian noise based adaptive extended and unscented Kalman filters and other estimation techniques such as particle filter will be employed and compared for precised backlash gap size estimation. In addition to conducting experiment to acquire relevant data for the estimation of coefficient of friction between mating gears, the visco-dynamic effect of a lubricant will also be taken into consideration. Moreover, a controller that compensates for the estimated backlash gap size shall be designed.

REFERENCES

[1] Q. Guan, L. Geng, S. Zhenghong, W. Yawen, M. Shangjun, and C. L. Teik, "A review of electromechanical actuators for more/all electric aircraft systems," *J. Mech. Eng. Sci.*, vol. 232, no. 22, Apr. 2017.
[2] A. C. Bertolino, A. De Martin, G. Jacazio, and M. Sorli, "Design and preliminary performance assessment of a PHM system for electromechanical flight control actuators," *Aerospace*, vol. 10, no. 4, p. 335, Mar. 2023.
[3] H. Ercan and M. Akin, "Performance analysis of electrical flight control actuation system in a commercial transport aircraft," *Aircr. Eng. Aerosp. Technol.*, vol. 94, no. 10, pp. 1671–1683, Dec. 2022.
[4] R. Hjelm, H. Hansson, A. Ahadi, C. Andersson, and J. Wahlström, "Influence of manufacturing error tolerances on contact pressure in gears," *Proc. Inst. Mech. Engineers, C, J. Mech. Eng. Sci.*, vol. 235, no. 20, pp. 5173–5185, Oct. 2021.
[5] Z. Tao, H. Chen, X. Zhang, and Y. Jiang, "Failure analysis of worm gear in worm transmission," *J. Phys., Conf. Ser.*, vol. 1965, no. 1, Jul. 2021, Art. no. 012132.
[6] K. J. Sharif, H. P. Evans, and R. W. Snidle, "Prediction of the wear pattern in worm gears," *Wear*, vol. 261, nos. 5–6, pp. 666–673, Sep. 2006.
[7] H. W. Carlos, "Gear backlash analysis of unloaded gear pairs in transmissions," 2016. [Online]. Available: https://api.semanticscholar.org/CorpusID:122853672
[8] A. Skulić, B. Stojanović, S. Radosavljević, and S. Veličković, "Experimental determination of worm gearing efficiency," *Appl. Eng. Lett., J. Eng. Appl. Sci.*, vol. 4, no. 4, pp. 115–119, 2019.
[9] G. Anusha, H. G. Rajath, and S. Prashanth, "A comprehensive review of condition monitoring techniques for gearboxes," *Int. J. Creative Res. Thoughts*, vol. 12, no. 8, pp. 515–522, 2024.
[10] K. Feng, J. C. Ji, Q. Ni, and M. Beer, "A review of vibration-based gear wear monitoring and prediction techniques," *Mech. Syst. Signal Process.*, vol. 182, Jan. 2023, Art. no. 109605.
[11] K. Feng, W. A. Smith, R. B. Randall, H. Wu, and Z. Peng, "Vibration-based monitoring and prediction of surface profile change and pitting density in a spur gear wear process," *Mech. Syst. Signal Process.*, vol. 165, Feb. 2022, Art. no. 108319.
[12] K. Feng, Q. Ni, and J. Zheng, "Vibration-based system degradation monitoring under gear wear progression," *Coatings*, vol. 12, no. 7, p. 892, Jun. 2022.
[13] A. Šmeringaiová, "Study vibration of worm gear boxes," *IOP Conf. Ser., Mater. Sci. Eng.*, vol. 1199, no. 1, Nov. 2021, Art. no. 012012.
[14] K. Feng, J. C. Ji, Y. Zhang, Q. Ni, Z. Liu, and M. Beer, "Digital twin-driven intelligent assessment of gear surface degradation," *Mech. Syst. Signal Process.*, vol. 186, Mar. 2023, Art. no. 109896.

[15] F. Susana, J. Andrés, M. Jon, N. Eva, F. Santiago, A. Andrés, and M. Esteban, "Health monitoring for electro-mechanical nose landing gear door actuator of a UAV, based on simulation modelling and data-driven techniques," *Chem. Eng. Trans.*, vol. 33, pp. 655–660, May 2013.
[16] R. Smid, "Digital twin for condition monitoring of actuators," in *Proc. 19th Int. Conf. Condition Monit. Asset Manag.*, 2023, pp. 1–5.
[17] M. Enis, P. Nedim, M. Adil, and D. Muamer, "A contact mechanics model for surface wear prediction of parallel-axis polymer gears," *Polymers*, vol. 16, no. 20, 2024, Art. no. 2858.
[18] M. Badr, P. Jerome, and G. Alexandre, "The backlash gap size estimation for electromechanical actuator in an operational behavior," in *Proc. Eur. Conf. Prognostic Health Manage. Soc.*, 2016, pp. 1–15.
[19] K. Bahdir, Y. Nihat, E. Fatih, and V. Mert, "A study on predicting and validating meshing gear pair backlash under various manufacturing and assembly errors," in *Proc. MATEC Web Conf.*, vol. 287, 2019, pp. 1–12.
[20] S. Christian, R. Michael, K. Robert, and D. André, "Automated measurement of backlash and stiffness in electro-mechanical flight control actuation," in *Recent Advances in Aerospace Actuation Systems and Components*, 2018.
[21] S. Sander-Tavallaey and K. Saarinen, "Backlash identification in transmission unit," in *Proc. IEEE Int. Conf. Control Appl.*, Jul. 2009, pp. 1325–1331.
[22] M. Nordin, J. Galic, and P.-O. Gutman, "New models for backlash and gear play," *Int. J. Adapt. Control Signal Process.*, vol. 11, no. 1, pp. 49–63, Feb. 1997.
[23] M. Nordin and P.-O. Gutman, "Controlling mechanical systems with backlash—A survey," *Automatica*, vol. 38, no. 10, pp. 1633–1649, Oct. 2002.
[24] J. Jaisheela and K. S. Kumar, "Control of backlash in electromechanical system-design and simulation based approach," in *Proc. Int. Conf. Devices, Circuits Syst. (ICDCS)*, Coimbatore, India, Mar. 2012, pp. 427–431.
[25] D. K. Prasanga, E. Sariyildiz, and K. Ohnishi, "Compensation of backlash for geared drive systems and thrust wires used in teleoperation," *IEEJ J. Ind. Appl.*, vol. 4, no. 5, pp. 514–525, 2015.
[26] R. Kalantari and M. S. Foomani, "Backlash nonlinearity modeling and adaptive controller design for an electromechanical power transmission system," *Trans. B, Mech. Eng.*, vol. 16, no. 6, pp. 463–469, 2009.
[27] M. Shoaib, M. Kim, D. Park, and J. Cheong, "Control of a worm-wheel gear driven rescue robot with friction compensation and its experimental verification," *Adv. Mech. Eng.*, vol. 15, no. 10, pp. 1–12, Oct. 2023.
[28] H. Kawasaki, S. Murakami, H. Kachi, and S. Ueki, "Novel climbing method of pruning robot," in *Proc. SICE Annu. Conf.*, Aug. 2008, pp. 160–163.
[29] D. C. May, S. Jayasuriya, and B. W. Mooring, "Modeling and control of a manipulator joint driven through a worm gear transmission," *J. Vibrat. Control*, vol. 6, no. 1, pp. 85–111, Jan. 2000.
[30] C. Unsal and P. K. Khosla, "Mechatronic design of a modular self-reconfiguring robotic system," in *Proc. Millennium Conf. IEEE Int. Conf. Robot. Autom. Symposia (ICRA)*, San Francisco, CA, USA, Apr. 2000, pp. 1742–1747.
[31] M. Zhang, C. Li, X. Wu, and Y. Zhu, "All-electric aircraft nose wheel steering system with two worm gears," *Trans. Nanjing Univ. Aeronaut. Astronaut.*, vol. 35, no. 1, pp. 170–180, 2018.
[32] C. Alexandru and C. Pozna, "Simulation of a dual-axis solar tracker for improving the performance of a photovoltaic panel," *Proc. Inst. Mech. Eng., A, J. Power Energy*, vol. 224, no. 6, pp. 797–811, Sep. 2010.
[33] H. G. Chothani and K. D. Maniya, "Experimental investigation of churning power loss of single start worm gear drive through optimization technique," *Mater. Today, Proc.*, vol. 28, pp. 2031–2038, Aug. 2020.
[34] W. Kacalak, M. Majewski, Z. Budniak, and J. Ponomarenkow, "Worm gear drives with improved kinematic accuracy," *Materials*, vol. 14, no. 24, p. 7825, Dec. 2021.
[35] K. Wojciech, M. Maciej, and B. Zbigniew, "Worm gear drives with adjustable backlash," *J. Mech. Robot.*, vol. 8, no. 1, 2016, Art. no. 014504.
[36] M. Elforjani, D. Mba, A. Muhammad, and A. Sire, "Condition monitoring of worm gears author links open overlay panel," *Appl. Acoust.*, vol. 73, no. 8, pp. 859–863, 2012.
[37] S. Raadnui, "Condition monitoring of worm gear wear and wear particle analysis of industrial worm gear sets," *Wear*, vol. 476, Jul. 2021, Art. no. 203687.
[38] H. Berkan, C. U. Rafet, O. Hasan, and K. Zeki, "Smart condition monitoring of worm gearbox," in *Proc. Inter-Noise*, Hamburg, Germany, 2016, pp. 6535–6544.
[39] A. Lagerberg and B. Egardt, "Backlash estimation with application to automotive powertrains," *IEEE Trans. Control Syst. Technol.*, vol. 15, no. 3, pp. 483–493, May 2007.
[40] J. Margielewicz, D. Gąska, and G. Litak, "Modelling of the gear backlash," *Nonlinear Dyn.*, vol. 97, no. 1, pp. 355–368, Jul. 2019.
[41] T.-J. Yeh and F.-K. Wu, "Modeling and robust control of worm-wheel gear-driven systems," *Simul. Model. Pract. Theory*, vol. 17, pp. 767–777, Jun. 2009.
[42] O. Pawel, A. Jan, and F. Michal, "Friction laws in modeling of dynamical systems," in *Modeling, Analysis and Control of Dynamical Systems With Friction and Impacts* (Nonlinear Science Series A). Singapore: World Scientific, 2017, p. 92.
[43] S. Sarkka, "Extended and unscented Kalman filtering," in *Bayesian Filtering and Smoothing*. Cambridge, U.K.: Cambridge Univ. Press, 2013.
[44] S. J. Julier and K. U. Jeffery, "A new extension of the Kalman filter to nonlinear systems," *Proc. SPIE*, vol. 3068, pp. 182–193, Jul. 1997.
[45] R. Turner and C. E. Rasmussen, "Model based learning of sigma points in unscented Kalman filtering," *Neurocomputing*, vol. 80, pp. 47–53, Mar. 2012.
[46] Kohara Gear Ind. *Easy Gear Selection Pages*. Accessed: Jul. 20, 2024. [Online]. Available: https://khkgears2.net/catalog5/
[47] M. C. VanDyke, J. L. Schwartz, and C. D. Hall, "Unscented Kalman filtering for spacecraft attitude state and parameter estimation," *Adv. Astron. Sci.*, vol. 118, pp. 217–228, Aug. 2004.

ABERA TULLU (Member, IEEE) received the Ph.D. degree in aerospace engineering from Pusan National University, South Korea, in 2017. He was a Postdoctoral Researcher with the Aerospace Engineering Department, Pusan National University, from March 2017 to February 2020, and an Assistant Professor of aerospace engineering with Sejong University, South Korea, from March 2020 to February 2023. He is currently a Research Associate with the Aerospace Engineering Department, Korea Aerospace University. His research interests include remotely piloted aircraft-based target tracking, path planning, obstacle avoidance, and aerial robot arm design and control.

JIHYOUNG CHA (Member, IEEE) received the B.S., M.S., and Ph.D. degrees from the Department of Aerospace and Mechanical Engineering, Korea Aerospace University, in 2012, 2014, and 2019, respectively. He is currently a Research Fellow with the Centre for Aeronautics, School of Aerospace, Transport and Manufacturing, Cranfield University, U.K. Previously, he was a Postdoctoral Researcher and Researcher with the Department of Computer Science, Electrical and Space Engineering, Luleå University of Technology, Sweden, from 2020 to 2023. His research interests include state estimation, system modeling and control, fault detection and diagnosis, and optimization.

SANGHO KO (Member, IEEE) received the Ph.D. degree from the Department of Mechanical and Aerospace Engineering, University of California San Diago (UCSD), in 2005. From 2005 to 2006, he was a Postdoctoral Scholar with UCSD, research system identification techniques. From March 2006 to February 2008, he was a Research Fellow with the Department of Electrical and Electronic Engineering, University of Melbourne, Australia, where he worked on finite sample quality assessment of system identification. From 1992 to 1999, he was with Samsung Aerospace Industries Ltd., Kyungnam, South Korea, where he was a Research and Development Engineer of digital flight control systems. He is currently a Professor with the School of Aerospace and Mechanical Engineering, Korea Aerospace University, South Korea. His research interests include state estimation and control, system identification, flight control, and propulsion system control.

DSPACE

https://dspace.org/

Modeling and simulation of backlash dynamics of worm-wheel system and its gap size estimation using Kalman filters

Tullu, Abera; Cha, Jihyoung; Ko, Sangho

2025-06-09
Institute of Electrical and Electronics Engineers (IEEE)
https://doi.org/10.1109/access.2025.3577747
Tullu A, Cha J, Ko S. (2025) Modeling and simulation of backlash dynamics of worm-wheel system and its gap size estimation using Kalman filters. IEEE Access, Volume 13, 2025, pp. 110779-110790

Downloaded from a DSpace repository. https://dspace.org/